Influence of the Surface Heating on Langmuir Circulation

HONG SIK MIN* AND YIGN NOH

Department of Atmospheric Sciences, Yonsei University, Seoul, Korea

(Manuscript received 25 August 2003, in final form 29 April 2004)

ABSTRACT

Large-eddy simulation of the oceanic mixed layer showed that Langmuir circulation (LC) is weakened under the surface heating and is ultimately broken down if the intensity of the surface heating becomes sufficiently strong. The critical condition for the breakdown of LC was mainly determined by the Hoenikker number Ho, and the transition occurs in the range Ho $\sim$ 1–2. The breakdown of LC leads to a drastic change in the characteristics of the oceanic mixed layer, such as the variation of the rms horizontal velocities with time, the ratio of the horizontal spectra of vertical velocity field, and the pitch. The stability condition for LC suggested by Leibovich was still observed in this simulation. Furthermore, it was found that LC is largely responsible for the formation of a thermocline and the maintenance of a well-mixed layer above it, and the depth of a thermocline was estimated in that case.

1. Introduction

There have been a large number of papers investigating Langmuir circulation (LC), including theoretical, numerical, and experimental studies, but many important aspects remain yet to be clearly understood (see, e.g., Pollard 1977; Leibovich 1983). Especially, we cannot predict properly how LC is modified by stratification and under which condition it breaks down, although it is expected to play a prominent role for the vertical transport of heat and momentum in the upper ocean.

Langmuir circulations are typically generated when the wind speed is larger than 3 m s^{-1}. The downward vertical velocity below the convergence region increases with the wind speed, sometimes exceeding 0.2 m s^{-1} (Weller and Price 1988). The downwind current at the surface is the strongest at the convergence region and has a magnitude comparable to the downwelling velocity (Smith et al. 1987; Weller and Price 1988).

Estimates of Langmuir cell spacing indicate a broad range of scales, from about 2 to 200 m (Plueddemann et al. 1996), and the maximum spacing is close to 2–3 times the mixed layer depth (Smith et al. 1987; Smith 1992). The streaks at the surface, the surface indications of Langmuir cells, are nearly oriented in the wind direction with the maximum angle less than 20°, and they often merge at characteristic Y junctions (Zedel and Farmer 1991; Thorpe 1992; Farmer and Li 1995).

The prevailing theory of LC is that of Craik and Leibovich (1976), which describes the formation of LC in terms of instability brought on by the interaction of the Stokes drift with the wind-driven surface shear current. The instability is initiated by an additional "vortex force" term in the momentum equation as $\mathbf{u}_s \times \boldsymbol{\omega}$, where $\mathbf{u}_s$ is the Stokes drift velocity and $\boldsymbol{\omega}$ is the vorticity.

Assuming a constant frictional velocity u_*, for surface waves with a characteristic wavenumber k and the Stokes drift velocity at the surface U_s, the occurrence of LC in a laminar flow with constant viscosity ν is determined by the Langmuir number La (Leibovich 1977a) defined by

$$\mathrm{La} = \left(\frac{k\nu}{u_*}\right)^{3/2}\left(\frac{2u_*}{U_s}\right)^{1/2}, \tag{1}$$

which represents a balance between the rate of diffusion of streamwise vorticity and the rate of production of streamwise vorticity by vortex stretching accomplished by the Stokes force. In the turbulent oceanic mixed layer, however, McWilliams et al. (1997) suggested a turbulent Langmuir number La_t as the relevant parameter

$$\mathrm{La}_t = (u_*/U_s)^{1/2}. \tag{2}$$

It is natural to expect that LC be affected by stratification in the mixed layer. Indeed, Weller and Price (1988) observed during Mixed Layer Dynamics Experiment (MILDEX) that LC was weaker under a stronger heat flux in May of 1983 than in December of 1982, although the strengths of the winds were about the same (see Fig. 9 in their paper). On the other hand, there also

* Current affiliation: Korea Ocean Research and Development Institute, Ansan, Korea.

Corresponding author address: Prof. Yign Noh, Department of Atmospheric Sciences, Yonsei University, Seoul 120-749, Korea.
E-mail: noh@atmos.yonsei.ac.kr

exist reports that the surface heating does not affect LC significantly under a certain condition (Harris and Lott 1973; Smith 1992).

Theoretical analysis for an inviscid, nonconducting fluid of infinite depth also suggests that LC cannot be maintained if

$$\mathrm{Ri}_* = \min\left[\frac{N^2(z)}{(\partial U/\partial z)(\partial U_s/\partial z)}\right] > 1, \tag{3}$$

where the Richardson number Ri_* is defined by the minimum over depth, N is the Brunt–Väisälä frequency, and U is the horizontal mean velocity (Leibovich 1977b). It is not yet clear, however, whether (3) can be applied in the real ocean.

It is thus interesting to clarify the effects of stratification on LC by taking advantage of recent advances in numerical simulation. The accurate prediction of the breakdown of LC is also imperative to understand the vertical transports of heat and momentum. For example, it has been reported that, when LC appears, it rapidly mixes away the near-surface stratification and redistributes heat vertically (Weller and Price 1988; Plueddemann and Weller 1999).

Based on numerical simulation results for a two-dimensional laminar flow, Li and Garrett (1995) proposed a criterion for the occurrence of LC in the oceanic mixed layer under the surface buoyancy flux B_0 in terms of La and the Hoenikker number

$$\mathrm{Ho} = 2B_0/(kU_s u_*^2), \tag{4}$$

which represents the relative importance of the buoyancy forcing over the vortex forcing. They suggested that LC is completely inhibited at Ho $\sim$ 2–4, which is beyond the range normally observed in the ocean. However, the validity of their conclusion is limited because it was obtained from a two-dimensional laminar flow whereas LC is essentially a three-dimensional turbulent flow.

There has been remarkable recent progress in turbulence simulation by using large-eddy simulation (LES), which is able to simulate the three-dimensional structure of turbulent flows realistically. There have been a few attempts to simulate LC in the oceanic mixed layer by using LES (Skyllingstad and Denbo 1995; McWilliams et al. 1997; McWilliams and Sullivan 2000; Skyllingstad 2000; Noh et al. 2004). However, there has been no systematic study yet to investigate the influence of the surface heating on LC by using LES.

Therefore, in this study we aim at understanding how the surface heating affects LC and predicting the criterion for the breakdown of LC, using LES. Moreover, we examine how the breakdown of LC affects the vertical mixing process in the oceanic mixed layer.

2. Model and experiments

The LES model we used in this study is developed based on the Parallelized LES Model (PALM), which has been extensively applied for the atmospheric boundary layer (Schröter et al. 2000; Raasch and Harbusch 2001; Weinbrecht and Raasch 2001; Noh et al. 2003a), the oceanic deep convection (Raasch and Etling 1998; Noh et al. 2003b), and the oceanic mixed layer (Noh et al. 2004). The model is based on the nonhydrostatic Boussinesq equations. Subgrid-scale turbulence is modeled according to Deardorff (1980), which is widely used in the LES of geophysical turbulent flows (Moeng 1984; Nieuwstadt and Brost 1986). Here a prognostic equation is solved for the subgrid-scale turbulent kinetic energy (TKE), which is used to parameterize the subgrid-scale fluxes.

The numerical scheme is a standard second-order finite-difference scheme using the absolutely conserving scheme of Piacsek and Williams (1970) for the nonlinear advection term. The prognostic equations are time-advanced by a leapfrog scheme. A weak time filter is applied to remove the time-splitting instability of the leapfrog scheme (Asselin 1972). During the integration, the time step is adjusted so that it never exceeds one-tenth of the allowed value due to the Courant–Friedrichs–Lewy (CFL) and diffusion criteria. Incompressibility is applied by means of the Poission equation for pressure, which is solved by the FFT method.

The code has recently been parallelized, and the performance of the new parallelized code is found to be excellent, with an almost linear speedup up to a very large number of processors; for example, the speedup is hardly different from the ideal case in the calculation with the size of grid points 160 × 160 × 64 using 256 processor elements of the Cray, Inc., T3E (Raasch and Schröter 2001).

For the application to the oceanic mixed layer, several modifications were made. A free-slip boundary condition was imposed at the surface. The momentum equation was modified by including a vortex force and an additional advection by the Stokes drift following the theory by Craik and Leibovich (1976), similar to McWilliams et al. (1997) and Skyllingstad and Denbo (1995) (see also Noh et al. 2004).

The box-filtered equation over the grid size of LES is then represented as

$$\frac{\partial u_i}{\partial t} + (u_j + u_{sj})\frac{\partial u_i}{\partial x_j} = -\frac{1}{\rho_0}\frac{\partial p}{\partial x_i} - \varepsilon_{ijk} f_j (u_k + u_{sk}) + \varepsilon_{ijk} u_{sj}\omega_k - b\delta_{i3} - \frac{\partial}{\partial x_j}\tau_{ij}, \tag{5}$$

where b is the buoyancy ($= -g\Delta\rho/\rho_0$), f is the Coriolis parameter, and τ_{ij} is the subgrid-scale Reynolds stress.

For simplicity, we assumed that both the wind stress and wave fields are in the x direction and further assumed that the wave field is steady and monochromatic. The associated Stokes velocity is then given by

$$u_s = U_s \exp(-2kz), \tag{6}$$

TABLE 1. Experimental parameters, such as the friction velocity u_*, the Stokes drift at the surface U_s, the wavelength λ ($=2\pi/k$), the Coriolis force f, and the corresponding turbulent Langmuir number La_t.

EXP	u_* (m s^{-1})	U_s (m s^{-1})	λ (m)	f ($\times$ 10^{-4} s^{-1})	La_t
A	0.01	0.082	80	1.2	0.35
B	0.01	0.082	40	1.2	0.35
C	0.01	0.195	40	1.2	0.23
D	0.01	0.05	80	1.2	0.45
E	0.005	0.082	80	1.2	0.25
F	0.01	0.082	80	0	0.35
G	0.01	0.082	40	0	0.35

with $U_s = (ak/2)^2(g/k)^{1/2}$, where a is the wave height and g is the gravitational acceleration.

The model domain was 300 m in the horizontal direction (x and y) and 80 m in the vertical direction (z) with a grid spacing of 2.5 m in both horizontal and vertical directions. The horizontal boundaries were periodic, and a free-slip boundary condition was applied at the bottom.

Initial experiments were carried out without surface heating with an initial density profile that was neutral up to 50 m and stable down below with a uniform buoyancy gradient $N^2 = 10^{-4}$ s^{-2}. The quasi-equilibrium state was reached after an 8-h integration; then a surface heating was imposed. A stable stratification below 50 m made it easier to reach a stationary state of LC, and the deepening rate of the mixed layer during the simulation ($\sim 10^{-4}$ m s^{-1}) was negligible in comparison with the velocity scale of LC.

Experiments with seven different combinations of u_*, U_s, $\lambda(=2\pi/k)$, and f were performed to investigate the role of each parameter (Table 1). We used the range $La_t \sim 0.2$–0.5, based on the observational evidence (Smith 1992). Analyses were made mainly on experiment (EXP) A (see Table 1). Different levels of buoyancy flux ($B_0 = 0$–10^{-6} m^2 s^{-3}) were imposed on each experiment, which corresponds to the heat flux 0–2700 W m^{-2} with the coefficient of thermal expansion 1.5×10^{-5} K^{-1}. Table 2 shows B_0 and the corresponding Ho for EXP A. The numbers following the name of a series of experiments denote the magnitude of B_0.

The subgrid-scale components of turbulent kinetic energy are much smaller than the resolved components in the present LES of the oceanic mixed layer (Noh et al. 2004), thus implying the insensitivity to the subgrid-scale parameterization.

3. Results

a. *Vertical velocity field under heating*

Figure 1 shows the instantaneous vertical velocity fields for different surface heating [B_0 = 0, 2, 6, 10 ($\times$ 10^{-7} m^2 s^{-3})] at horizontal cross sections at increasing depths (z = 2.5, 7.5, 12.5, and 17.5 m). Hereinafter, all figures in this article are based on the results 2 h after the onset of the heat flux unless stated otherwise.

TABLE 2. Surface buoyancy flux B_0 and the corresponding Hoenikker number Ho for EXP A.

EXP	B_0 ($\times$ 10^{-7} m^2 s^{-3})	Ho
A0	0	0
A1	1	0.31
A2	2	0.62
A4	4	1.24
A6	6	1.86
A8	8	2.48
A10	10	3.10

In the absence of heat flux (Fig. 1a), general features of the simulation results are similar to those of the previous LES by Skyllingstad and Denbo (1995) and McWilliams et al. (1997). Near the surface, the solution is dominated by streaks of small spacing of a few meters oriented approximately along the wind direction. With increasing depths, however, streaks of larger spacing up to 200 m, which are oriented diagonal to the wind direction, increasingly dominate. The multiple-scale pattern of LC, as shown here, has also been observed in the field (Thorpe 1992; Pluddemann et al. 1996).

The maximum spacing of Langmuir cells is close to 2–3 times the mixed layer depth, and the downwelling velocity reaches up to 0.04 m s^{-1}, which is also in good agreement with the field observations (Smith et al. 1987; Smith 1992; Plueddemann et al. 1996).

It can be easily seen in the figures that LC is increasingly weakened with increasing heat flux (Figs. 1b–d). In the case of the largest surface heating (EXP A10), the pattern of LC cannot be discerned any more.

The weakening of LC under the influence of the surface heating is also identified in the vertical cross sections of instantaneous vertical velocity fields (Fig. 2). Strong downward jets associated with LC are clearly observed up to a depth of the mixed layer (z = 50 m) in the absence of the surface heating (EXP A0). We can also notice that the maximum downward velocities are found around the middepth of the mixed layer, in agreement with observations (Weller and Price 1988).

In EXP A2, the penetration depth of LC is reduced to less than 20 m as a result of the formation of a thermocline under the stabilizing buoyancy flux (see Fig. 7). In EXPs A6 and A10, no discernible downward jets are observed. It is interesting, however, to find that the level of TKE near the surface is higher in EXP A10 than in EXP A6, which is due to the stronger shear in the former case (see Fig. 8).

In general, patterns from other experiments are not significantly different from EXP A. The LC penetrates less deeply when k is larger (EXP B), and the streaks of all scales are aligned along the wind direction at all depths in the absence of the Coriolis force (EXPs F and G).

b. *Variation of the rms horizontal velocities with time*

Contrary to the case of a two-dimensional laminar flow considered by Li and Garrett (1995), it is difficult

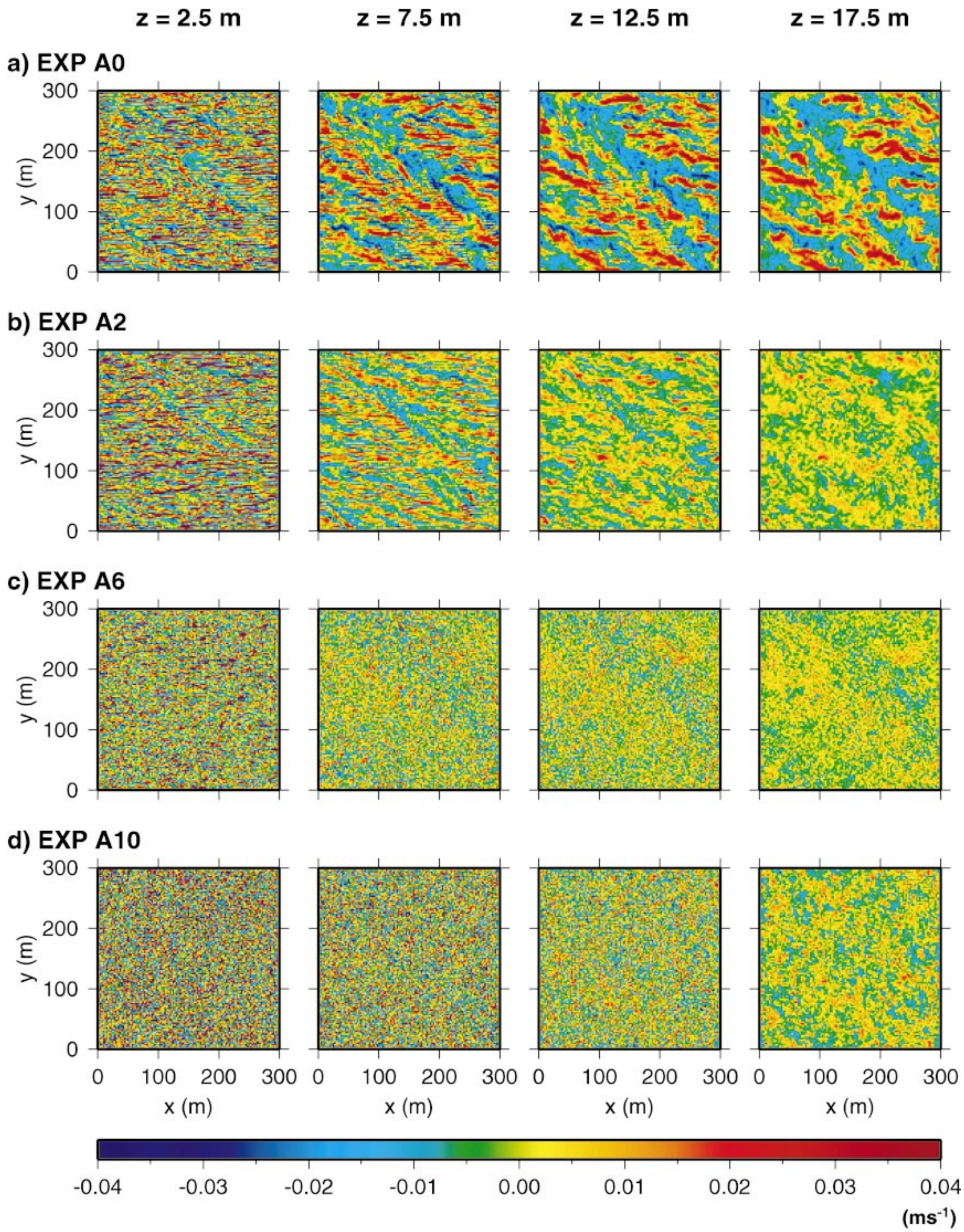

FIG. 1. Instantaneous vertical velocity fields at the horizontal cross sections $z = 2.5$, 7.5, 12.5, and 17.5 m at 2 h after the onset of the surface heat flux (positive value indicates downward): (a) EXP A0, (b) EXP A2, (c) EXP A6, and (d) EXP A10.

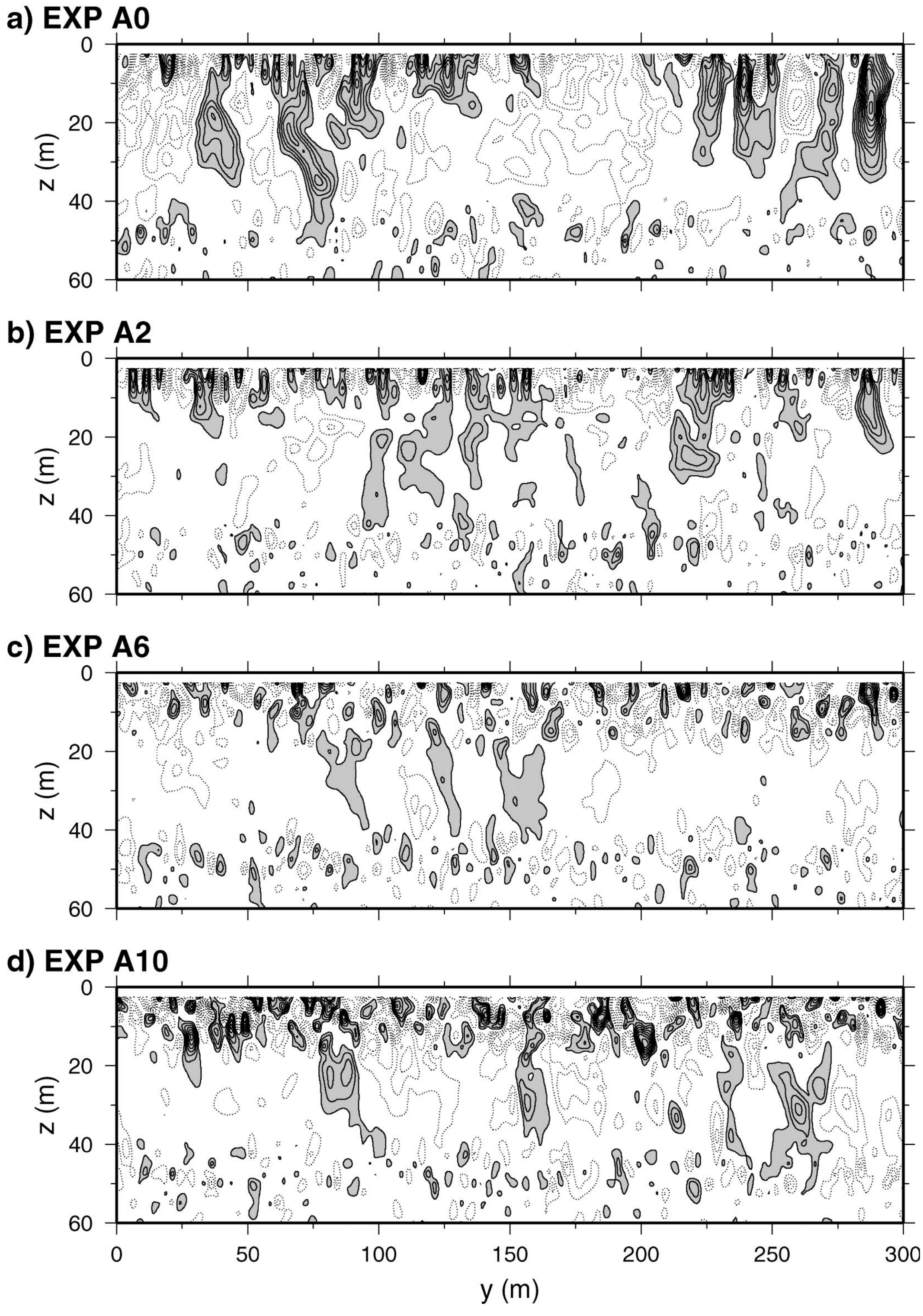

FIG. 2. Instantaneous vertical velocity fields for (a) EXP A0, (b) EXP A2, (c) EXP A6, and (d) EXP A0 at the vertical cross section $x = 150$ m. Contour levels are 0.005 m s^{-1}. Solid lines represent the downward velocity, and dotted lines represent the upward one. Here the regions in which the downward velocity exceeds 0.005 m s^{-1} are shaded.

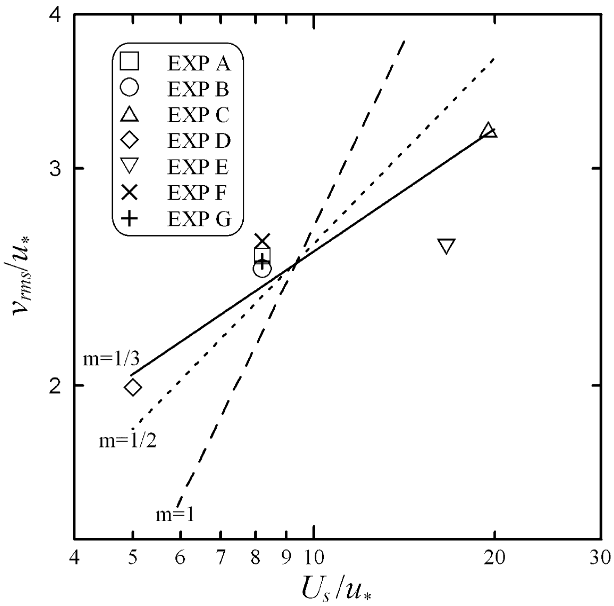

FIG. 3. Root-mean-square crosswind velocities vs Stokes drift at the surface, scaled by u_*, in the homogeneous oceanic mixed layer before the onset of the heat flux. The solid, dotted, and dashed lines denote $m = 1/3$, $1/2$, and 1, respectively, for $v_{rms}/u_* \propto (U_s/u_*)^m$.

to measure the maximum downwelling velocity objectively in the present case with turbulent downward jets of various size and intensity. Therefore, we calculated the rms velocity perpendicular to the wind at the surface, v_{rms}, which is equivalent to the convergent velocity scale associated with LC.

For the estimation of v_{rms}, various values have been suggested for m in the relation $v_{rms}/u_* \propto (U_s/u_*)^m$ such as $m = 1/3$, $1/2$, or 1, based on theoretical arguments or the analysis of observation data (Pluddemann et al. 1996; Smith 1996, 1998). The LES result, shown in Fig. 3, suggests a better agreement with $m = 1/3$, which also corresponds with the LES results by Skyllingstad (2000).

The variation of v_{rms} is examined to investigate the influence of surface heating on the strength of LC (Fig. 4a). It decreases with time under the surface heating, and the decreasing rate increases with increasing B_0, when $B_0 \leq 4 \times 10^{-7}$ m^2 s^{-3} (EXPs A1, A2, and A4). However, if $B_0 \geq 8 \times 10^{-7}$ m^2 s^{-3} (EXPs A8 and A10), it starts to increase after the initial period of decreasing. The case of EXP A6 shows a somewhat intermediate pattern.

Meanwhile, the rms velocity in the windward direction at the surface, u_{rms}, decreases with time, when $B_0 \leq 6 \times 10^{-7}$ m^2 s^{-3} (EXPs A1, A2, A4, and A6), but it increases when $B_0 \geq 8 \times 10^{-7}$ m^2 s^{-3} (EXPs A8 and A10) (Fig. 4b).

From a closer examination of the vertical velocity fields in Fig. 1 and 2, we could find that the two regimes of contrasting pattern in the temporal variations of v_{rms} and u_{rms} shown above coincide with the cases in which LC is maintained or destroyed, respectively.

The above results imply that the surface heating weakens LC until it reaches a critical value, thus decreasing both v_{rms} and u_{rms} that are mainly due to LC. However, if B_0 becomes larger than a critical value, LC cannot be maintained any more, and a stronger shear appears with time owing to the inhibition of the downward momentum flux (see Fig. 7 and 8). In this case, the values of v_{rms} and u_{rms}, which are not related to LC, increase with time as a result of the increased horizontal TKE.

c. *The ratio of the horizontal spectra of vertical velocity field*

As mentioned in section 3a, one of the most significant features of LC observed from the LES results is that LC is composed of multiple scales and that the small-scale cells along the wind direction dominate near the surface. This feature suggests that there may exist an asymmetry between the spectra of vertical velocity variation in the downwind and crosswind directions near the surface.

Figure 5 compares the ratio of the horizontal spectra of the vertical velocity field near the surface ($z = 2.5$ m) between the downwind and crosswind directions (Φ_{wx}/Φ_{wy}). The ratio Φ_{wx}/Φ_{wy} decreases with increasing wavenumber in the presence of LC (EXPs A0, A1, A2, and A4), consistent with the pattern of LC mentioned above. On the other hand, in the absence of LC (EXPs A8 and A10) the spectra in two different directions remain almost the same regardless of the wavenumber.

d. *Variation of the pitch*

One of the key parameters that represent the intensity of LC is the pitch, the ratio of the surface downwind jet strength to the maximum downwelling velocity w_{dn} (Li and Garrett 1995), that is,

$$\mathrm{Pt} = \frac{u_{conv} - u_{div}}{w_{dn}}, \tag{7}$$

where u_{conv} and u_{div} are the downwind velocity at the convergent and divergent zones, respectively. Once again, it is difficult to calculate the pitch by (7) in the present simulation, and therefore we obtained scatter plots of $w(z = 5$ m) versus $u(z = 0$ m) instead (Fig. 6).

They show that a significant correlation exists between u and w in the presence of LC (EXPs A0 and A2), but it disappears once LC is broken down (EXP A10). The value of Pt during EXPs A0 and A2 can be estimated as Pt $\sim$ 1–2 from the slopes of the correlations, if $w(z = 5$ m) is used for w_{dn}. However, the real value of Pt must be smaller, because $w(z = 5$ m) is less than w_{dn}.

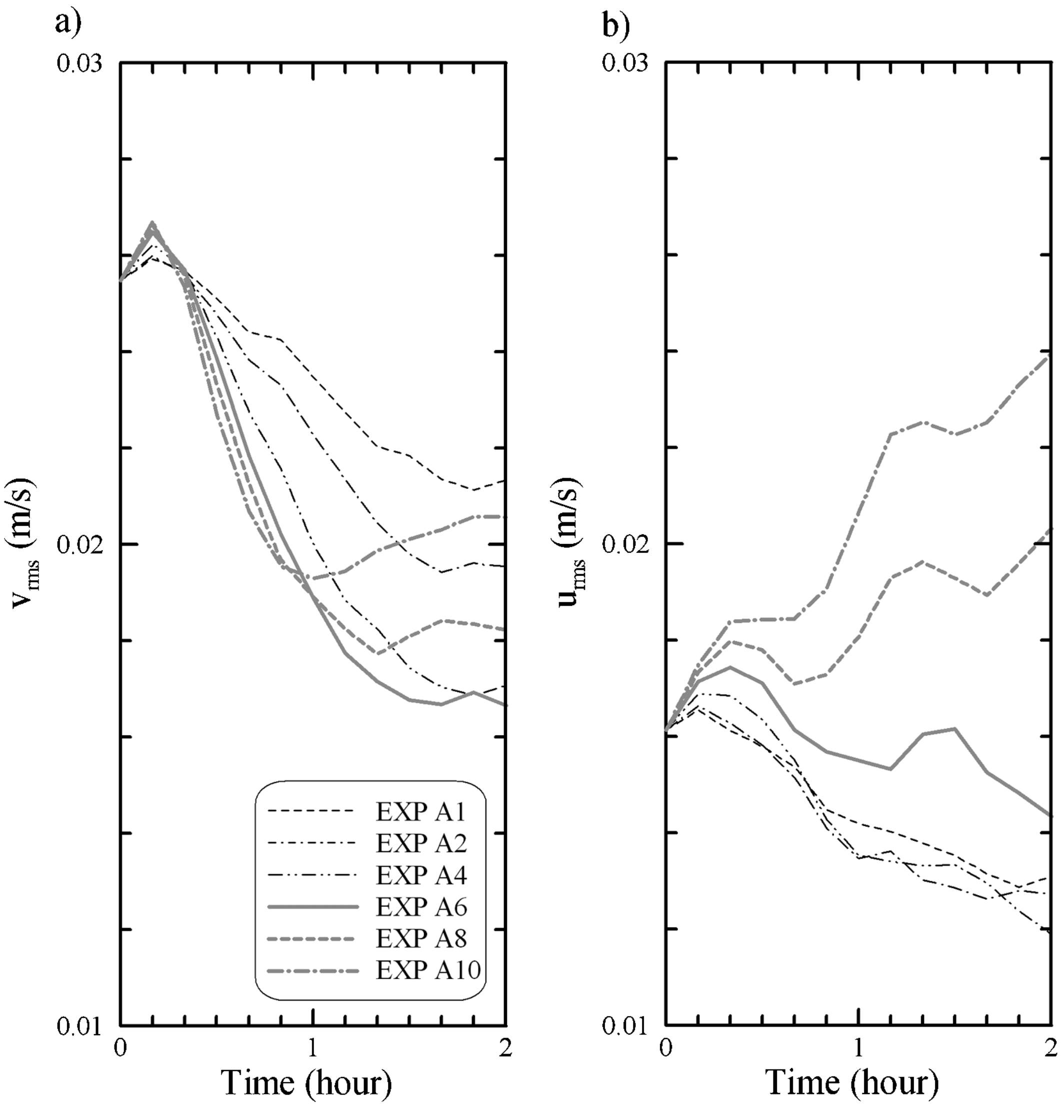

FIG. 4. Temporal variations of rms horizontal turbulent velocities from EXP A: (a) the crosswind velocity v_{rms}, and (b) the downwind velocity u_{rms}.

e. Evolution of profiles of buoyancy and horizontal velocity under heating

It is expected that LC plays a significant role in the vertical mixings of heat and momentum in the oceanic mixed layer. In particular, Plueddemann and Weller (1999) observed that the upper ocean did not stratify in response to diurnal heating when LC was sustained, whereas strong stratification appeared near the surface in the absence of LC. We should expect the similar drastic change in the vertical profiles of temperature and velocity from our LES results, depending on whether or not the breakdown of LC occurs.

Figure 7 shows the evolution of profiles of horizontal-mean buoyancy under different surface buoyancy fluxes. In the presence of LC (EXP A2), a thermocline is formed with time at a certain depth and a relatively well-mixed layer is maintained above it. On the other hand, strong stratification appears near the surface without forming a thermocline in the absence of LC (EXP A10), as in the case of the atmospheric boundary layer. The results are in accord with field observations by Plueddemann and Weller (1999). They are also consistent with the fact that the level of TKE near the surface becomes much higher in the presence of LC in the oceanic mixed layer under a stabilizing buoyancy flux (Skyllingstad and Denbo 1995).

In a similar way, profiles of horizontal-mean horizontal velocities reveal a substantial increase of the vertical shear near the surface in the absence of LC (Fig. 8), which leads to the enhancement of the TKE level near the surface as indicated in Figs. 2 and 4.

Noh (1996) suggested that in the oceanic mixed layer

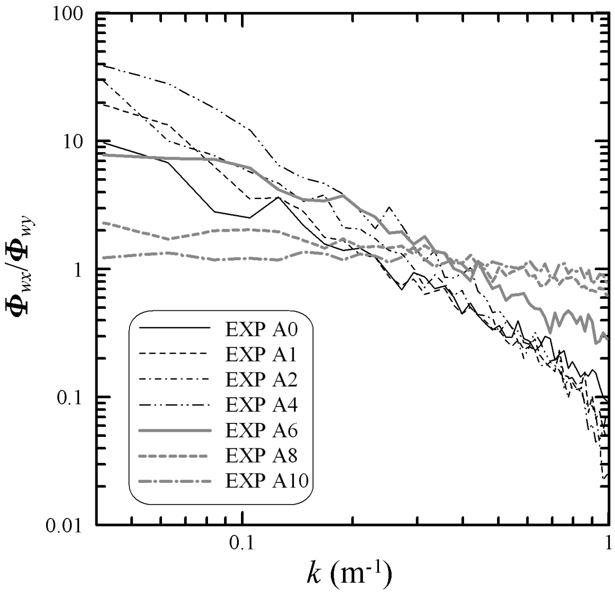

FIG. 5. The ratio of the horizontal spectra of the vertical velocity field near the surface (z = 2.5 m) between the downwind and crosswind directions (Φ_{wx}/Φ_{wy}).

under the stabilizing buoyancy flux the formation of a thermocline at a certain depth while maintaining a well-mixed layer above it is due to the strong mixing near the surface by wave breaking. The present result reveals, however, that LC also plays an important role for it, as suggested earlier by Langmuir (1938) himself.

f. Evolution of Ri$_*$

Here we examine whether the condition (3), $\mathrm{Ri}_* > 1$, suggested by Leibovich (1977b), for the breakdown of LC in an inviscid, nonconducting fluid of infinite depth can be observed in the present LES results.

The time series of Ri_* shows that Ri_* grows larger than about 1 in the case in which LC is broken down (EXPs A8 and A10) but that in the case in which LC is maintained (EXPs A1, A2, and A4) Ri_* remains invariant with time at a value of less than 1 after about 10 min from the onset of the heat flux (Fig. 9). It implies that the stability condition $\mathrm{Ri}_* > 1$ can be still observed even in the more realistic turbulent flows, although the transition to the breakdown of LC occurs gradually.

g. Criterion for the breakdown of LC

We have found so far that there exist various contrasting characteristics of the oceanic mixed layer responding to the surface heat flux, depending on whether or not LC is present. By carefully examining these various features, that is, the view of vertical velocity fields, variations of the rms horizontal velocities with time, the ratio of the horizontal spectra of vertical velocity field, the pitch, the profiles of buoyancy and horizontal velocity, and the evolution of Ri_*, we were able to determine a criterion for the breakdown of LC, based on the data from a series of experiments (EXPs A–G).

We can expect that the pattern of the oceanic mixed layer affected by the surface buoyancy flux and the Stokes force is determined by u_*, B_0, U_s, k, and f, or

$$F(u_*, U_s, B_0, k, f) = 0. \tag{8}$$

Dimensional analysis of (8) in terms of u_* and k leads to

$$F(\mathrm{La}_t, \mathrm{Ho}, u_*k/f) = 0, \tag{9}$$

where the last term in (9) represents the ratio of the Ekman layer depth ($\sim u_*/f$) to the penetration depth of the Stokes drift ($\sim k^{-1}$).

Figure 10 shows a regime diagram for the criterion for the breakdown of LC in terms of La_t and Ho. The transitional state, denoted by symbols with slant lines, represents the intermediate case in which the various characteristics mentioned above could not be clearly identified with either case. It shows that the breakdown of LC is largely determined by Ho. The critical Hoenniker number Ho_c, at which the transition occurs, lies in the range $\mathrm{Ho}_c \sim 1$–2. It is somewhat smaller than the value $\mathrm{Ho}_c \sim 2$–4 suggested by Li and Garrett (1995) for the complete breakdown of LC. The value of Ho in the LES by Skyllingstad and Denbo (1995), in which LC was still observed, was 0.188.

The dependence on La_t is not important, however, within the range of La_t in the present simulation. Note also that the value of La_t in the ocean does not go beyond the range of the present simulation normally. The results from EXPs F and G are similar to those from EXPs A and B, which suggests that the breakdown of LC is not sensitive to the Coriolis force, or u_*k/f, either.

Meanwhile, there appears a tendency in Fig. 10 that the values of Ho_c are slightly smaller for the experiments with larger k (EXPs B and C). This result is certainly not due to the effects of u_*k/f, as mentioned above. It is suspected that the vortex forcing might be estimated more appropriately by $kU_su_*^2e^{-2kz}$ at a certain depth z below the surface rather than $kU_su_*^2$ used in (4), and thus a more appropriate representation of the ratio between the buoyancy forcing and the vortex forcing may be better represented by $e^{2kz}\mathrm{Ho}$ rather than Ho.

h. The depth of the surface mixed layer

As shown in Fig. 7, in the presence of LC the surface heat flux imposed on the sea surface leads to the formation of a thermocline while a well-mixed layer is maintained above it.

The resultant mixed layer depths are shown in Fig. 11. For a more accurate estimation of the depth of a thermocline, we imposed a passive tracer flux at the surface for 10 s after 1 h of the onset of the surface heating. The depth of the thermocline D, or the mixed

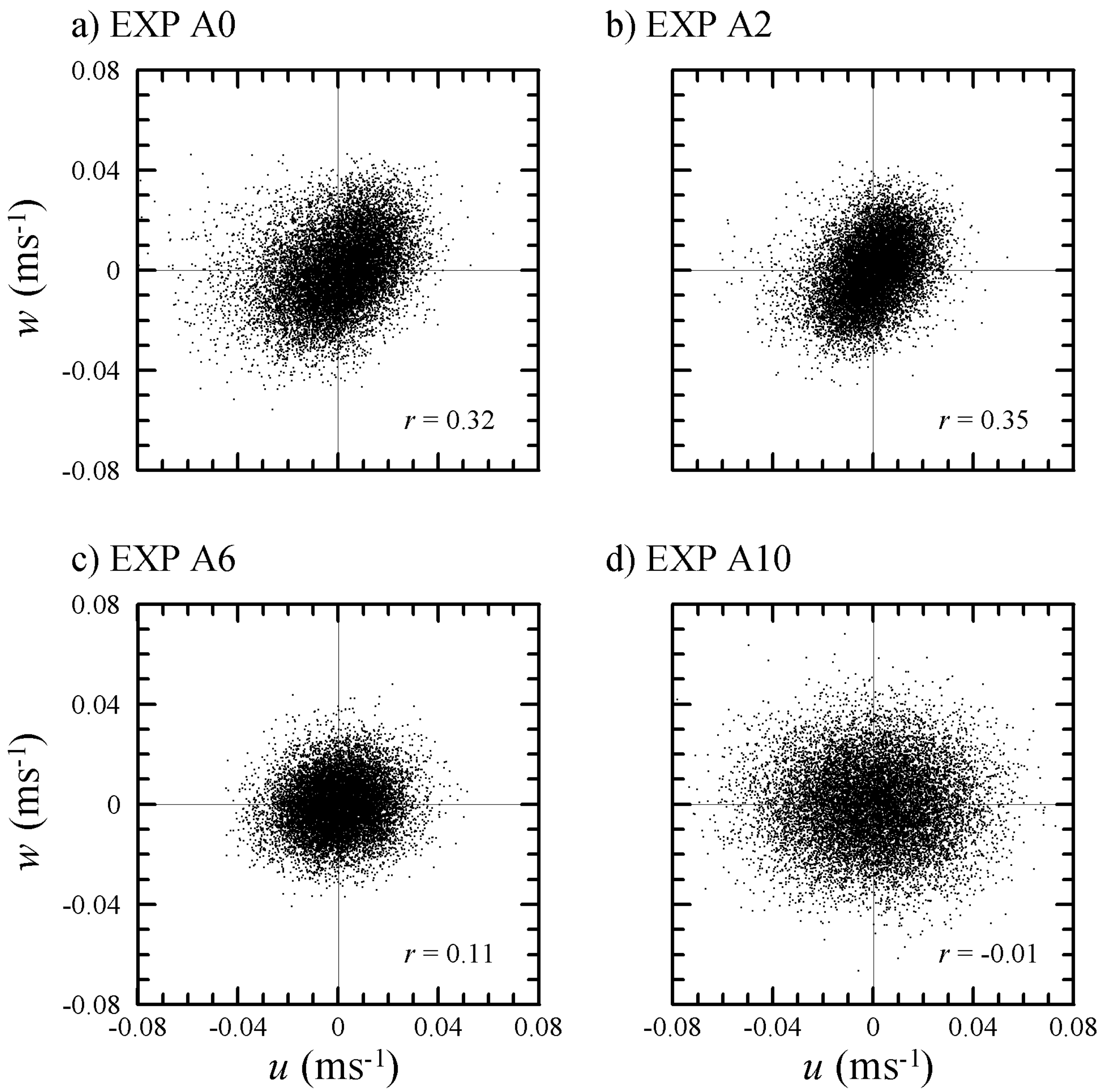

FIG. 6. The scatterplot of downwelling velocities ($z = 5$ m) vs downwind velocities ($z = 0$ m) (here r represents the correlation coefficient): (a) EXP A0, (b) EXP A2, (c) EXP A6, and (d) EXP A10.

layer depth, was then defined as the depth at which the concentration becomes 90% of that at the surface at 1 h after the introduction of the tracer.

It has been suggested that the depth of a thermocline formed responding to the stabilizing buoyancy flux at the surface in the oceanic mixed layer increases with the Monin–Obukhov length scale $L = u_*^3/B_0$ (Kitaigorodskii 1970; Noh 1996).

In the presence of LC, however, the maximum downwelling velocity w_{dn} may be a more relevant parameter, rather than u_*, for the vertical mixing process in the mixed layer, as suggested by Li et al. (1995). Using the relations $w_{dn} \sim \upsilon_{rms}$ and $\upsilon_{rms} \sim (u_*^2 U_s)^{1/3}$ (see Fig. 3), we can expect that D can be scaled as a function of $L_* = u_*^2 U_s/B_0$.

Figure 11 shows the increase of the depth of a thermocline according to L_*, consistent with the hypothesis given above. It is also observed, however, that D tends to be larger for the cases with smaller k. It appears to be natural, because LC penetrates deeper with smaller k. It is also found that D is affected by f at larger depths, and thus it becomes larger in the case $f = 0$.

4. Concluding remarks

In this paper, we performed the first systematic attempt to investigate the response of the surface heating on LC in the oceanic mixed layer using LES. The analyses of the LES results not only confirmed the various

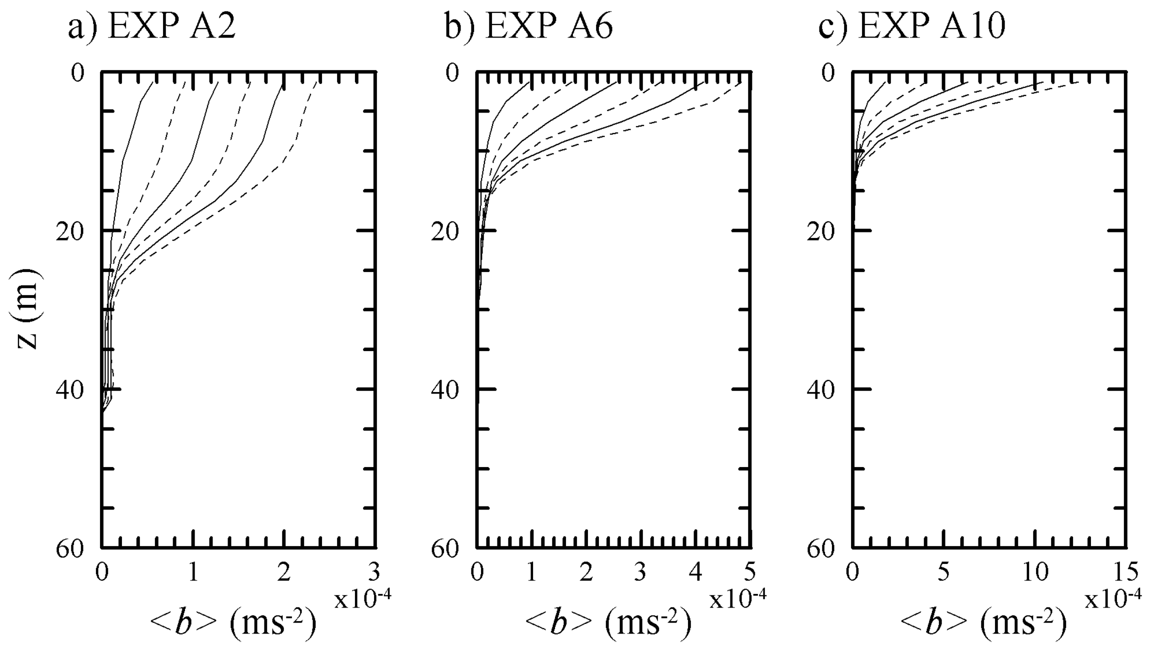

FIG. 7. Evolution of horizontal-mean buoyancy profiles with time under the stabilizing buoyancy flux: (a) EXP A2, (b) EXP A6, and (c) EXP A10 (Δt is 1 h for EXP A2 and 20 min for EXPs A6 and A10).

reported features of the observed LC, but also gave new insight into the nature of LC.

We have found that LC is weakened with increasing surface buoyancy flux B_0 and is ultimately broken down if B_0 becomes sufficiently large. The critical condition for the breakdown of LC was mainly determined by Ho [$=2B_0/(kU_s u_*^2)$]. The critical Hoenniker number Ho_c, at which the transition occurs, lies in the range $\mathrm{Ho}_c \sim 1$–2.

It is important to note, however, that wave breaking always occurs in the real ocean, whereas it is not included in the present simulation. The recent LES study reveals that the presence of wave breaking does not modify LC significantly, but it weakens LC slightly (Noh et al. 2004), which implies that Ho_c can be slightly smaller.

The wind stress and maximum heat flux during

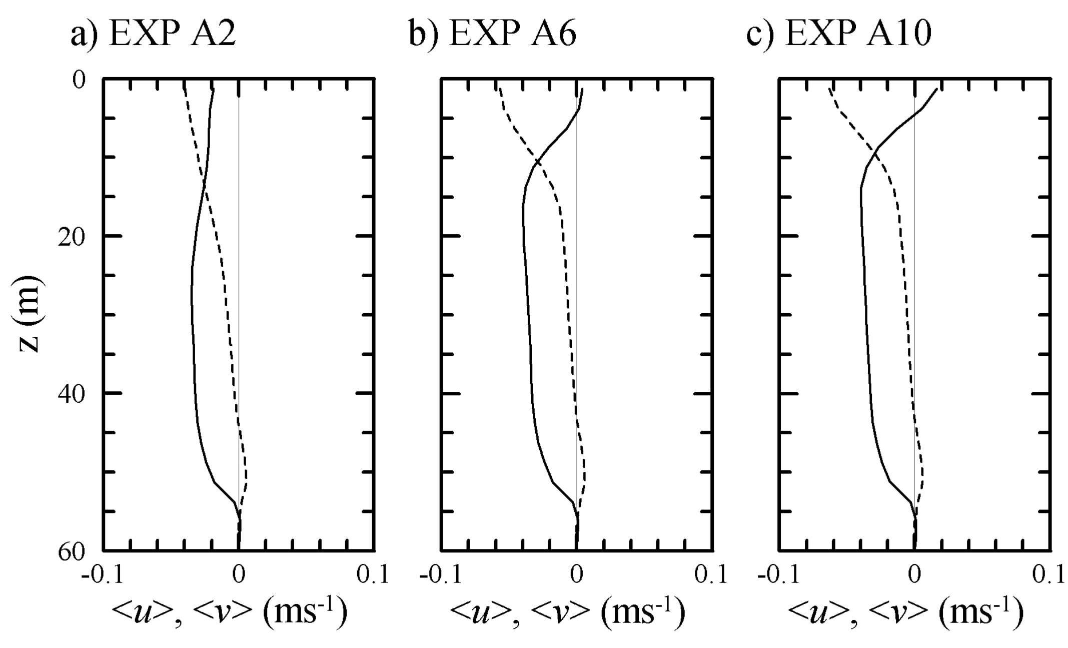

FIG. 8. Horizontal-mean horizontal velocity profiles: (a) EXP A2, (b) EXP A6, and (c) EXP A10. Solid and dashed lines denote along-wind and crosswind components, respectively.

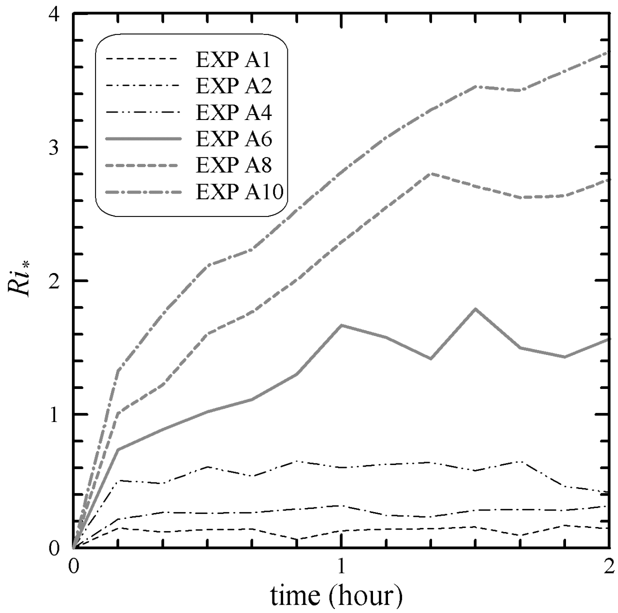

FIG. 9. Temporal variation of Ri_* for EXP A.

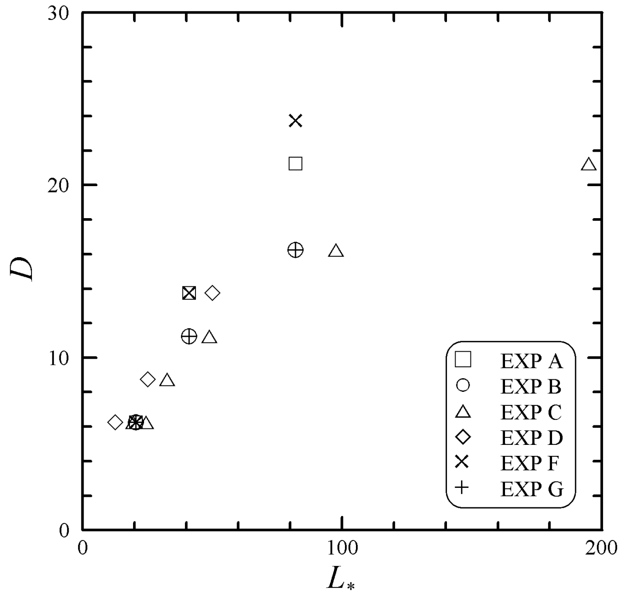

FIG. 11. Mixed layer depth D vs L_* ($=u_*^2U_s/B_0$). Only the cases of D larger than 5 m are plotted.

MILDEX, in which the stronger and weaker LCs were observed under weaker and stronger heat fluxes as mentioned in section 1, can be roughly represented by $u_* \sim 0.01$ m s^{-1} and $B_0 \sim 2 \times 10^{-7}$–$4 \times 10^{-7}$ m^2 s^{-3} (Weller and Price 1988). The corresponding Ho is then roughly estimated as Ho $\sim$ 0.2–0.5, if we assume typical values such as $U_s \sim 10u_*$ and $\lambda(=2\pi/k) \sim 40$ m. Nonetheless, more systematic observation data are required for a proper comparison between numerical results and observation data.

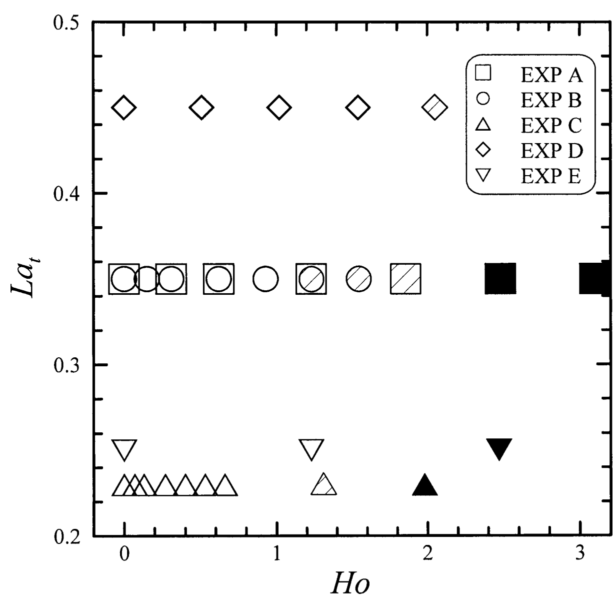

FIG. 10. A regime diagram for the breakdown of LC. Open and closed symbols denote the cases of the occurrence and no occurrence of LC, respectively. Slanted symbols denote the transitional cases.

We also have found that the structure of the oceanic mixed layer and the vertical mixing process change radically along with the breakdown of LC—for example, variations of the rms horizontal velocities with time, the ratio of the horizontal spectra of vertical velocity field, the pitch, and the profiles of buoyancy and horizontal velocity. We also found that the stability condition for LC suggested by Leibovich (1977b) for an inviscid, nonconducting fluid of infinite depth [see (3)] is still observed in the present simulation, although the transition is gradual.

It is now evident that LC plays a critical role for the vertical mixing process in the oceanic mixed layer, in which it is responsible for the formation of a thermocline and the maintenance of the mixed layer. The more accurate prediction of the occurrence of LC and its intensity, including the case of the unstable mixed layer, is imperative to improve our understanding of the mixing process in the near-surface layer of the ocean.

Acknowledgments. This work was supported by the Korea Research Foundation (KRF-2003-015-C00684), in which main calculations were performed by using the supercomputing resources of the KISTI. We are grateful to Dr. Siegfried Raasch, University of Hannover, for his help in developing the code and preparing the manuscript. We are also grateful to Dr. K. Bryan, Princeton University, for his valuable comments on the manuscript.

REFERENCES

Asselin, R., 1972: Frequency filter for time integrations. *Mon. Wea. Rev.*, **100,** 487–490.

Craik, A. D. D., and S. Leibovich, 1976: A rational model for Langmuir circulations. *J. Fluid Mech.,* **73,** 401–426.
Deardorff, J. W., 1980: Stratocumulus-capped mixed layers derived from a three-dimensional model. *Bound.-Layer Meteor.,* **18,** 495–572.
Farmer, D. M., and M. Li, 1995: Patterns of bubble clouds organized by Langmuir circulation. *J. Phys. Oceanogr.,* **25,** 1426–1440.
Harris, G. P., and J. N. A. Lott, 1973: Observations of Langmuir circulations in Lake Ontario. *Limnol. Oceanogr.,* **18,** 584–589.
Kitaigorodskii, S. A., 1970: *The Physics of Air–Sea Interaction.* Israel Program for Scientific Translations, 237 pp.
Langmuir, I., 1938: Surface motion of water induced by wind. *Science,* **87,** 119–123.
Leibovich, S., 1977a: On the evolution of the system of wind drift currents and Langmuir circulations in the ocean. Part 1. Theory and averaged current. *J. Fluid Mech.,* **79,** 715–743.
——, 1977b: Convective instability of stably stratified water in the ocean. *J. Fluid Mech.,* **82,** 561–581.
——, 1983: The form and dynamics of Langmuir circulation. *Annu. Rev. Fluid Mech.,* **15,** 391–427.
Li, M., and C. Garrett, 1995: Is Langmuir circulation driven by surface waves or surface cooling? *J. Phys. Oceanogr.,* **25,** 64–76.
——, K. Zahariev, and C. Garrett, 1995: Role of Langmuir circulation in the deepening of the ocean surface mixed layer. *Science,* **270,** 1955–1957.
McWilliams, J. C., and P. P. Sullivan, 2000: Vertical mixing by Langmuir circulation. *Spill Sci. Technol. Bull.,* **6,** 225–237.
——, ——, and C. H. Moeng, 1997: Langmuir turbulence in the ocean. *J. Fluid Mech.,* **334,** 1–30.
Moeng, C.-H., 1984: A large-eddy-simulation model for the study of planetary boundary-layer turbulence. *J. Atmos. Sci.,* **41,** 2042–2062.
Nieuwstadt, F. T. M., and R. A. Brost, 1986: The decay of convective turbulence, *J. Atmos. Sci.,* **43,** 532–546.
Noh, Y., 1996: Dynamics of diurnal thermocline formation in the ocean mixed layer. *J. Phys. Oceanogr.,* **26,** 2183–2195.
——, W. G. Cheon, S. Y. Hong, and S. Raasch, 2003a: Improvement of the *K*-profile model layer based on large eddy simulation data. *Bound.-Layer Meteor.,* **107,** 401–427.
——, ——, and S. Raasch, 2003b: The role of preconditioning on the onset of open-ocean deep convection. *J. Phys. Oceanogr.,* **33,** 1145–1166.
——, H. S. Min, and S. Raasch, 2004: Large eddy simulation of the ocean mixed layer: The effects of wave breaking and Langmuir circulation. *J. Phys. Oceanogr.,* **34,** 720–735.
Piacsek, S. A., and G. P. Williams, 1970: Conservation properties of convection difference schemes. *J. Appl. Meteor.,* **9,** 856–861.
Plueddemann, A., and R. A. Weller, 1999: Structure and evolution of the oceanic surface boundary layer during the Surface Waves Processes Program. *J. Mar. Res.,* **21,** 85–102.
——, J. A. Smith, D. M. Farmer, R. A. Weller, W. R. Crawford, R. Pinkel, S. Vagle, and A. Gnanadesikan, 1996: Structure and variability of Langmuir circulation during the Surface Waves Processes Program. *J. Geophys. Res.,* **101,** 3525–3543.
Pollard, R. T., 1977: Observations and theories of Langmuir circulations and their role in near surface mixing. *A Voyage of Discovery: George Deacon 70th Anniversary Volume,* M. Angel, Ed., Pergamon, 235–251.
Raasch, S., and D. Etling, 1998: Modeling deep ocean convection: Large eddy simulation in comparison with laboratory experiments. *J. Phys. Oceanogr.,* **28,** 1786–1802.
——, and G. Harbusch, 2001: An analysis of secondary circulations and their effects caused by small-scale surface inhomogeneities using large-eddy simulation. *Bound.-Layer Meteor.,* **101,** 31–59.
——, and M. Schröter, 2001: A large eddy simulation model performing on massively parallel computers. *Meteor. Z.,* **10,** 363–372.
Schröter, M., J. Bange, and S. Raasch, 2000: Simulated airborne flux measurements in a LES generated convective boundary layer. *Bound.-Layer Meteor.,* **95,** 437–465.
Skyllingstad, E. D., 2000: Scales of Langmuir circulation generated using a large-eddy simulation model. *Spill Sci. Technol. Bull.,* **6,** 239–246.
——, and D. W. Denbo, 1995: An ocean large-eddy simulation of Langmuir circulations and convection in the surface mixed layer. *J. Geophys. Res.,* **100,** 8501–8522.
Smith, J. A., 1992: Observed growth of Langmuir circulation. *J. Geophys. Res.,* **97,** 5651–5667.
——, 1996: Observations of Langmuir circulation, waves, and the mixed layer. *The Air–Sea Interface: Radio and Acoustic Sensing, Turbulence, and Wave Dynamics,* M. A. Donelan, W. H. Hui, and W. J. Plant, Eds., University of Toronto Press, 613–622.
——, 1998: Evolution of Langmuir circulation during a storm. *J. Geophys. Res.,* **103,** 12 649–12 668.
——, R. Pinkel, and R. A. Weller, 1987: Velocity structure in the mixed layer during MILDEX. *J. Phys. Oceanogr.,* **17,** 425–439.
Thorpe, S., 1992: The break-up of Langmuir circulation and the instability of an array of vortices. *J. Phys. Oceanogr.,* **22,** 350–360.
Weinbrecht, S., and S. Raasch, 2001: High resolution simulations of the turbulent flow in the vicinity of an Arctic lead. *J. Geophys. Res.,* **106,** 27 035–27 046.
Weller, R. A., and J. F. Price, 1988: Langmuir circulation within the oceanic mixed layer. *Deep-Sea Res.,* **35,** 711–747.
Zedel, L., and D. M. Farmer, 1991: Organized structures in subsurface bubble clouds: Langmuir circulation in the open ocean. *J. Geophys. Res.,* **96,** 8889–8900.